Experimental Analysis and Computational Modeling of Residual Stress in β -Ga₂O₃ Thin Films Grown on Si by RF Magnetron Sputtering

A. Revenko^{a,*}, V. Kidalov^{b,c}, D. Duleba^a, M. Derhachov^d, R. Redko^e, R.P. Johnson^a, M.-A. Assmann^b, O. Gudymenko^e, O. Sushko^d and M. Koptiev^d

Received: 25.06.2025 & Accepted: 26.09.2025

Doi: 10.12693/APhysPolA.148.158 *e-mail: andy.revenko@gmail.com

Gallium oxide is becoming increasingly attractive as a next-generation material for semiconductor applications, prompting the need for efficient and economical techniques for thin-film fabrication, especially on non-native substrates. In this work, β -Ga₂O₃ films with a thickness of 0.25 μ m were grown on a silicon substrate via radio-frequency magnetron sputtering. Raman spectroscopy and X-ray diffraction analysis confirmed the good crystalline quality of the synthesized β -Ga₂O₃ films. The mechanical stresses in the β -Ga₂O₃/Si heterostructure were measured using X-ray diffraction. A comparative analysis with simulated data obtained via finite element modeling demonstrated good correlation between experiment and theory.

topics: Ga₂O₃ and Si, Raman spectroscopy, mechanical stress, radio-frequency (RF) magnetron sputtering

1. Introduction

Gallium oxide (Ga_2O_3) is one of the key wide-bandgap materials in the development of next-generation semiconductor devices. Its bandgap ranges from 4.5 to 5.3 eV, depending on the crystalline structure. Moreover, gallium oxide exhibits excellent optical, structural, and electrical properties [1–3]. Ga_2O_3 thin films have been successfully implemented in various semiconductor devices, including lithium batteries [4], gas sensors [5–7], metal—oxide—semiconductor field-effect transistors (MOSFETs) [8–10], metal—semiconductor field-effect transistors (MESFETs) [2, 11], and Schottky barrier diodes (SBDs) [2, 12, 13].

Additionally, there is considerable interest in deep ultraviolet photodetectors, capacitors based on metal-oxide-semiconductor (MOS) [14], and improving solar cell performance [7, 15–18]. The

 β -phase of Ga_2O_3 is especially noteworthy because of its exceptional optical transparency in the ultraviolet and visible wavelengths [11, 19–21].

Various methods are employed for the deposition of ${\rm Ga_2O_3}$ films, including metal-organic vapor phase epitaxy (MOVPE) [22, 23], halide vapor phase epitaxy (HVPE) [24, 25], molecular beam epitaxy (MBE) [26, 27], metal-organic chemical vapor deposition (MOCVD) [28, 29], pulsed laser deposition (PLD) [30, 31], mist-chemical vapor deposition (mist-CVD) [32, 33], and radiofrequency magnetron sputtering [34–36]. Among these techniques, radio-frequency (RF) magnetron sputtering is considered as an accessible and cost-effective method, which has been employed in this study for the epitaxial growth of ${\rm Ga_2O_3}$ films.

The most commonly used substrates for Ga_2O_3 film deposition include Ga_2O_3 , SiO_2 glass, Al_2O_3 , MnO, SiC, and Si [2, 20, 33, 36–38]. Although

^a School of Chemistry, University College Dublin, Belfield, Dublin 4, D04 N2E5, Dublin, Ireland ^b Experimentelle Physik 2, Technische Universitat Dortmund, Otto-Hahn-Straße 4a, 44227, Dortmund, Germany

^cDmytro Motornyi Tavria State Agrotechnological University, B. Khmelnytsky Ave 18, 72312, Melitopol, Ukraine

^dOles Honchar Dnipro National University, Nauky Ave 72, 49010, Dnipro, Ukraine

 $[^]e$ V.E. Lashkaryov Institute of Semiconductor Physics NAS of Ukraine, Nauky Ave 45, 02000 Kyiv, Ukraine

sapphire is widely used, its dielectric properties limit its application in β -Ga₂O₃-based electronic devices. In contrast, silicon has been well studied and extensively utilized in electronic devices, making it a promising substrate for the deposition of β -Ga₂O₃ films. Silicon substrates are not only costeffective and widely available but are also compatible with various optoelectronic applications. However, the structural and lattice parameter differences between silicon and gallium oxide present challenges in forming perfect crystalline β -Ga₂O₃ films. To address these issues, this study proposes the deposition of β -Ga₂O₃ films on Si substrates using RF magnetron sputtering as a method known for its affordability and scalability.

In our previous study, we investigated the structural and electrical properties of gallium oxide films grown on Si substrates [39]. Si(100) substrates with a porous surface layer were used in order to partially compensate residual mechanical stresses that occur in Ga₂O₃/Si structures during cooling to room temperature due to differences in lattice parameters and material properties (thermal expansion coefficient, Young's modulus, and Poisson's ratio). In the present work, we used monocrystalline Si(111) substrates without a porous surface layer. This choice was also supported by previous reports that highlighted the advantages of the Si(111) orientation for β -Ga₂O₃ film growth, showing favorable structural properties compared to Si(100) substrates [40, 41]. Based on these results, the use of Si(111) was considered the most appropriate for investigating residual stress in β -Ga₂O₃/Si heterostructures.

Since residual stress in heterostructures can strongly degrade their structural, electrical, and optical properties [42, 43], this study focuses on quantifying stress in β -Ga₂O₃/Si structures. The novelty of this work lies in combining experimental and theoretical stress evaluation via finite element analysis (using COMSOL) of β -Ga₂O₃ films grown on Si substrates. While the present model provides a first-order approximation, its further development can serve as a predictive tool for optimizing deposition parameters, enabling the fabrication of high-quality β -Ga₂O₃ films with minimal residual mechanical stress.

2. Experimental methods

 Ga_2O_3 films were deposited on Si(111) substrates using RF magnetron sputtering with a 99.999% Ga_2O_3 target. The deposition was conducted in a high-purity argon atmosphere at a chamber pressure of 2 mTorr for 110 min. The substrates were maintained at $473~\rm K$ throughout the process. Following the deposition, the sample was annealed at $1073~\rm K$ (800°C) for two hours in air with a heating/cooling rate of about $6^{\circ}\rm C/min$.

Scanning electron microscopy (SEM) was performed using a TESCAN MIRA3 IMU system (TESCAN, Czech Republic) with an In-Beam detector operating at 10.0 kV.

Raman analysis was conducted to assess the phase composition and crystalline quality of the ${\rm Ga_2O_3}$ thin films. The measurements were carried out in quasi-backscattering geometry using a HORIBA Jobin Yvon T64000 triple spectrometer integrated with an Olympus BX41 microscope. The experimental measurements were conducted at room temperature using a 532 nm line from a diodepumped solid-state (DPSS) laser (Spectra-Physics).

X-ray diffraction (XRD) analysis was conducted in Bragg–Brentano geometry using a Philips X'Pert PRO MRD diffractometer equipped with a $\text{Cu}K_{\alpha 1}$ source ($\lambda = 1.5406$ Å) operating at an anode voltage of 45 kV and a current of 40 mA. Phase identification was performed using the HighScore software package (Malvern Panalytical).

Numerical simulations of stress distribution were performed using COMSOL Multiphysics. The model was based on the "Solid Mechanics" module combined with the "Linear Elastic Materials" domain and "Thermal Expansion" attribute. Stress values, including stress tensors and von Mises stress, were extracted from the central region of the model to minimize boundary effects. This approach showed good agreement with both the literature and experimental XRD results.

3. Results and discussion

3.1. Characterization of morphology

Figure 1 shows scanning electron microscopy (SEM) images of the cross-section of the $\rm Ga_2O_3/Si$ sample. A sharp interface between the $\rm Ga_2O_3$ film and monocrystalline Si substrate is clearly visible.

The $\rm Ga_2O_3$ film exhibited a uniform thickness of ≈ 250 nm across the entire cross-section. These observations indicate that the selected RF magnetron sputtering parameters enabled a uniform $\rm Ga_2O_3$ film growth process.

3.2. X-ray analysis

Figure 2 shows the diffractogram of the $\rm Ga_2O_3/Si$ sample. The black curve corresponds to measurements performed in grazing incidence geometry, whereas the red curve represents those acquired using symmetric geometry. The $\rm Ga_2O_3$ film is formed on Si with an orientation of the (111) planes to the surface, as a strong (111) reflex is observed at 2 Theta = 28.42° (Fig. 2, red curve). The diffraction peaks of the $\rm Ga_2O_3$ phase are relatively broad. Full-profile analysis using the Rietveld method in

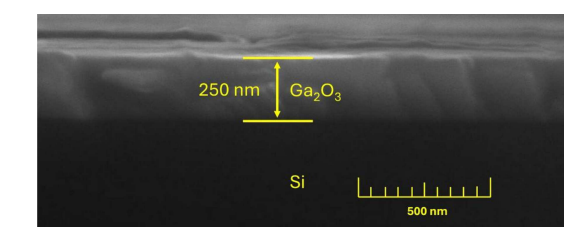


Fig. 1. SEM images of the cross-section of the Ga_2O_3/Si sample (voltage 10.0 kV, view field 2.0 μ m, magnitude 94.7kx).

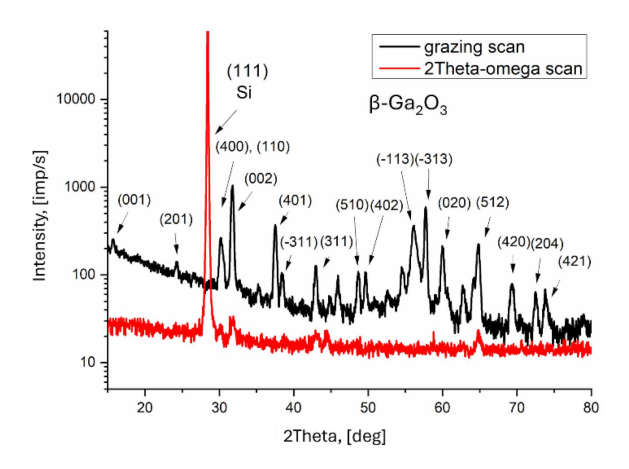


Fig. 2. Diffractogram of β -Ga₂O₃/Si (black curve — grazing incidence geometry, red curve — symmetric geometry).

the HighScore Plus software allowed the refinement of the monoclinic Ga_2O_3 lattice parameters to a=12.2177 Å, b=3.0430 Å, and c=5.7989 Å.

The coherent scattering domain size, determined by the Williamson–Hall method, was estimated to be D=27.4 nm, with an average microstrain (ε) of 0.11%. This calculation was based on the following equation [44, 45]

$$\beta \cos(\theta) = \lambda/D + 4\varepsilon \sin(\theta), \tag{1}$$

where θ represents the Bragg angle, and β is the full width at half maximum (FWHM) of the corresponding (hkl) diffraction peaks.

The residual mechanical stress in the β -Ga₂O₃ film was calculated using the uniaxial approach. Considering a Young's modulus (E) of 198 GPa determined via high-precision nanoindentation [46, 47], the stress (σ) was calculated as follows

$$\sigma = E \,\varepsilon,\tag{2}$$

where σ is the stress value, and E and ε are the Young's modulus and microstrain, respectively.

The average microstrain ε of 0.11% is significantly smaller than the value of 0.17% obtained in our previous work [39], indicating that the use of Si(111) substrates allows for the reduction of residual stress even without employing an additional porous surface layer.

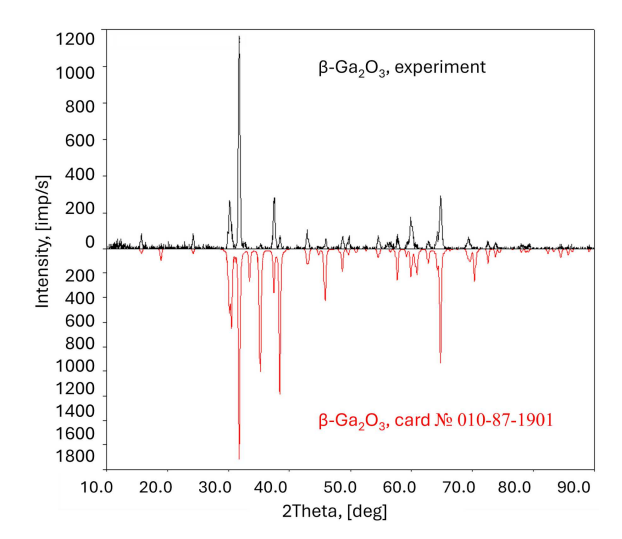


Fig. 3. Diffractogram of β -Ga₂O₃/Si (black curve — experimental sample, red curve — reference data (data card no. 010-87-1901)).

The estimated stress value is approximately $\sigma=0.2$ GPa, which is consistent with or slightly lower than the values reported in the literature [39, 48, 49]. These results confirm the formation of a β -modification gallium oxide film with good structural quality, in agreement with previous studies [50–54].

Additional XRD measurements were performed to evaluate the correspondence with the reference data for unstrained β -Ga₂O₃, and the results are shown in Fig. 3. The diffractogram of the sample exhibited only the polycrystalline β -Ga₂O₃ phase. As shown in Fig. 3, all prominent peaks of the experimental sample (black curve) coincide with those of the data card no. 010-87-1901 for the β -Ga₂O₃ phase (inverted red curve).

Thus, it can be concluded that the β -Ga₂O₃ films obtained in this study exhibited good crystallographic quality with low residual mechanical stresses.

3.3. Raman spectroscopy

Monoclinic β -Ga₂O₃ belongs to space group C2/m. Theoretical group analysis classifies the phonon modes of β -Ga₂O₃ according to $\Gamma_{\rm opt}=10{\rm Ag}+5{\rm Bg}+4{\rm Au}+8{\rm Bu}$. The Ag and Bg symmetries are Raman-active phonon modes, whereas Au and Bu are infrared-active [55]. Figure 4 shows the Raman scattering spectrum of Ga₂O₃/Si.

The basic vibrational modes of β -Ga₂O₃ are grouped into three frequency intervals: high-frequency of $> 500~\rm cm^{-1}$, medium-frequency of $300-500~\rm cm^{-1}$, and low-frequency of $100-300~\rm cm^{-1}$. The high-frequency modes, i.e., Ag(8)–Ag(10) and Bg(5), correspond to the stretching and bending

TABLE I

Raman peaks position [cm⁻¹] for β -Ga₂O₃ films in this work and for reference data for unstrained β -Ga₂O₃ samples from the literature [52, 54, 57, 58]. Values in parentheses indicate the difference between the measurements in this work and the literature data.

	T					
Raman	Rama	man peaks position (difference relative to reference data) $[\operatorname{cm}^{-1}]$				
$oxdot{mode}$	Current work	Ref. [57]	Ref. [54]	Ref. [58]	Ref. [52]	
Ag(1)	_	111	_	110.2	111.0	
Bg(1)	_	114	_	113.6	114.8	
$\mathrm{Bg}(2)$	143.7	147 (-3.3)	142 (1.7)	144.7 (-1.0)	144.8 (-1.1)	
Ag(2)	169.5	169 (0.5)	167 (2.5)	169.2 (0.3)	169.9 (-0.4)	
Ag(3)	199.8	199 (0.8)	198 (1.8)	200.4 (-0.6)	200.2 (-0.4)	
Ag(4)	318.5	318 (0.5)	$320 \ (-1.5)$	318.6 (-0.1)	$320.0 \; (-1.5)$	
Ag(5)	344.4	346 (-1.6)	344 (0.4)	346.4 (-2.0)	$346.6 \; (-2.2)$	
Bg(3)	_	353	_	_	353.2	
Ag(6)	415.5	415 (0.5)	415 (0.5)	415.7 (-0.2)	416.2 (-0.7)	
Ag(7)	_	475	473	_	474.9	
Bg(4)	_	_	_	473.5	474.9	
Ag(8)	_	628	627	628.7	630.0	
$\mathrm{Bg}(5)$	651.7	651 (0.7)	_	_	$652.3 \; (-0.6)$	
Ag(9)	_	657	651	652.5	658.3	
Ag(10)	_	763	765	763.9	766.7	

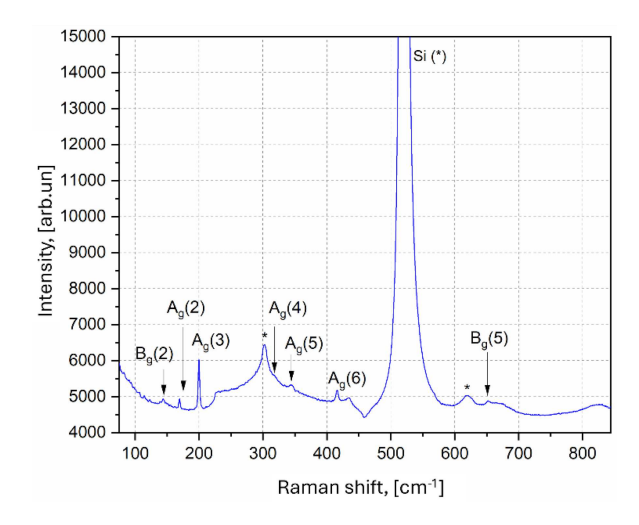


Fig. 4. Raman scattering spectra of β -Ga₂O₃/Si.

vibrations of GaO_4 tetrahedra. The medium-frequency modes, i.e., Ag(4)–Ag(7), are attributed to the deformation of Ga_2O_6 octahedra. The low-frequency modes, namely Ag(1)–Ag(3), Bg(1), and Bg(2), are associated with the libration and translation of tetrahedra–octahedra chains, providing insights into long-range lattice periodicity [48, 54–57].

The experimental spectrum contains peaks from all three intervals: Bg(2), Ag(2), and Ag(3) in the low-frequency range; Ag(4), Ag(5), and Ag(6) in the medium-frequency range; and Bg(5) in the high-frequency range.

Thus, Raman spectroscopy confirmed that the synthesized Ga_2O_3 films exhibited a β -phase. Table I compares our measurement results with reference data for bulk samples reported in the literature [52, 54, 57, 58]. The maximum absolute difference between our data and the literature is 3.3 cm⁻¹, while the maximum average difference is 1.775 cm^{-1} (Bg(2) peak). These discrepancies with reference data are acceptable, considering that Raman emission peaks in Ga₂O₃ can exhibit redshifts [54] of up to 20 cm⁻¹ and blueshifts [55] of up to 40 cm⁻¹. Consequently, the Raman spectroscopy results are in good agreement with the XRD measurements, confirming that the Ga₂O₃ films possess the β -phase and correlate well with the reference data.

Although Raman scattering can, in principle, be used for strain analysis, in our case the spectrum does not exhibit the complete set of peaks reported in the literature. Combined with the diversity of interpretations found in the literature regarding Raman peak shifts in β -Ga₂O₃ [49, 56], this limits the possibility of quantitative stress evaluation. Furthermore, comparison between XRD and Raman results is inherently difficult, since XRD yields an average value over the entire film thickness, whereas Raman spectroscopy measures stress locally at the laser spot. Therefore, in this work, Raman spectroscopy is used primarily to confirm the β -phase and to qualitatively assess crystalline quality, while quantitative stress values were derived from XRD analysis.

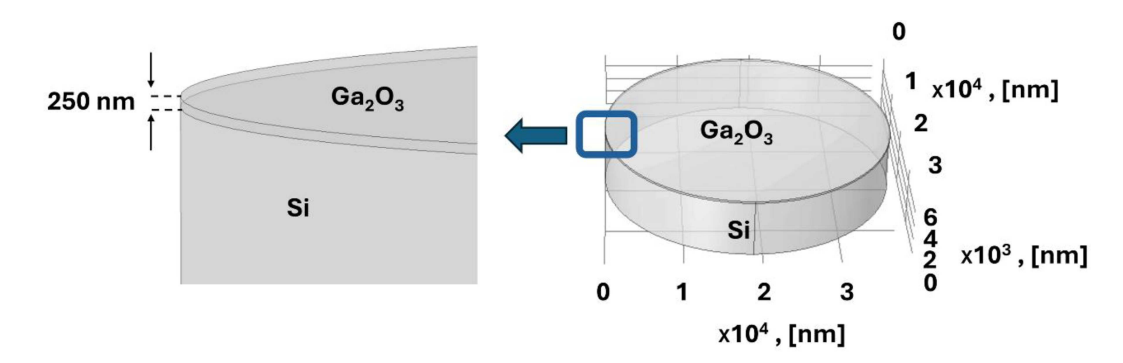


Fig. 5. Ga_2O_3/Si structure, where its radius is 18.75 μ m, Si substrate thickness is of 7.5 μ m, and Ga_2O_3 film thickness is 250 nm.

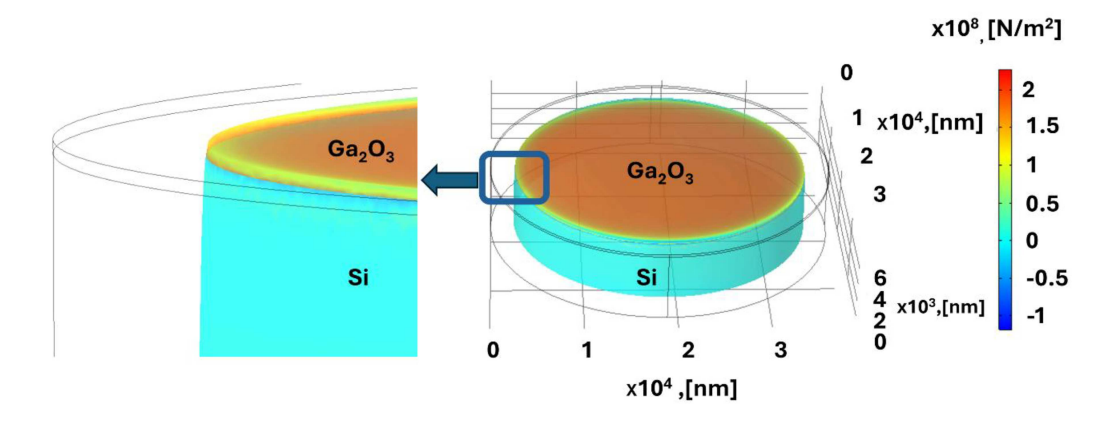


Fig. 6. Simulation results for the stress tensor (Gauss point evaluation) in the ${\rm Ga_2O_3/Si}$ structures .

3.4. Simulation of a residual stress in β -Ga₂O₃/Si structures

This section presents finite element simulation results for residual stress in β -Ga₂O₃ thin films grown on silicon substrates, comparing theoretical estimates with experimental data. The simulation is based on material-specific parameters such as thermal expansion coefficient (TEC), Young's modulus, Poisson's ratio, and density for both β -Ga₂O₃ and the silicon substrate.

We previously utilized a similar model to calculate the stress values in SiC/porous-Si/Si structures, which showed good agreement with the data from XRD and Raman spectroscopy analysis [59]. We have also calculated stress values in SiC/Si, as this structure can be compared to reports in the literature, and Gusev et al. [60] conducted a quantitative and qualitative estimation of SiC film relaxation on both mono- and porous-Si substrates.

The purpose of the simulation was not to model the growth process of the ${\rm Ga_2O_3}$ film itself, but rather to evaluate the residual stresses that develop during the cooling of the entire heterostructure from the annealing temperature down to room temperature. The modeling approach was based on the "Solid Mechanics" interface, complemented by the

TABLE II Material parameters for $\beta\text{-Ga}_2\mathrm{O}_3$ and Si based on reference literature.

	Units	${ m Ga_2O_3}$	Si
TEC	$[K^{-1}] \times 10^{-6}$	1.54-3.54	2.59-2.63
Young's	[Pa] ×10 ⁹	120-241	130-185
$ootnote{ ext{modulus}}$		120 241	130 100
Poisson's		0.29-0.31	0.26-0.28
ratio		0.29 0.51	0.20 0.20
Density	$[{ m kg/m^3}]$	5880-6000	2330
Refs.		[43, 47, 61–63]	[60, 64-67]

"Linear Elastic Materials" domain and the "Thermal Expansion" attribute. To suppress rigid body motion, the domain constraint "Rigid Body Suppression" was applied, ensuring numerical stability with a minimum set of constraints. Stresses were assumed to arise solely from the difference between the annealing temperature and room temperature, reflecting the thermal mismatch between Ga_2O_3 and Si as described by their material parameters: thermal expansion coefficient, density, Young's modulus, and Poisson's ratio. The analysis was performed as a stationary (time-independent) study.

The Ga₂O₃/Si interface was treated as perfectly bonded, which is consistent with the sharp interface observed experimentally.

A cylindrical geometry was adopted as the most symmetric and illustrative representation, while computational constraints required limiting the overall model dimensions. Stress evaluation was carried out in the central region of the film, where boundary effects are negligible. This approach provided stress values in close agreement with both experimental measurements and literature data. Future refinements will involve a time-dependent model that can account for cooling rates and additional technological parameters.

SEM characterization determined the uniform film thickness and confirmed the quality of the ${\rm Ga_2O_3/Si}$ interface. In addition, XRD and Raman spectroscopy provided clear evidence that the deposited films correspond to the β -modification of ${\rm Ga_2O_3}$, with no additional phases detected. These results support the assumption of structural homogeneity adopted in the finite element modeling.

For the work herein, the range of reported values for the material properties of Si and β -Ga₂O₃ is summarized in Table II (see also [43, 47, 60–67]). We have utilized TEC values of $3.54 \times 10^{-6} \; \rm K^{-1}$, Young's modulus of 198 GPa, Poisson's ratio of 0.31, and density of 5880 kg/m³ for Ga₂O₃ in our model. For the Si substrate, we have based on the following parameters: TEC values of $2.6 \times 10^{-6} \; \rm K^{-1}$, Young's modulus of 180 GPa, Poisson's ratio of 0.26, and density of 2330 kg/m³.

The thickness of the β -Ga₂O₃ film obtained from the experimental data was found to be 250 nm. For the present model, we assumed the thickness (z-axis) and radius (x- and y-axis) of the entire Ga₂O₃/Si structure to be 7.75 μ m and 18.75 μ m, respectively. Due to computational constraints, the dimensions of the simulated domain were limited accordingly. The geometry used in the simulation is illustrated in Fig. 5.

Simulations predicted a residual stress of ≈ 0.22 GPa in the β -Ga₂O₃ layer, which is in good agreement with the 0.2 GPa value obtained from XRD analysis. Figure 6 shows the distribution of mechanical stress in the Ga₂O₃/Si structure based on stress tensor values evaluated at Gauss points. The results indicate that the β -Ga₂O₃ film experiences tensile stress (positive values), whereas the Si substrate undergoes compressive stress (negative values).

The simulation results for the β -Ga₂O₃/Si structures at 0.22 GPa are in good agreement with the experimental data from XRD analysis, which shows a value of 0.2 GPa, which is significantly less than or close to the data provided in the literature [54, 55].

In future work, we plan to refine the model geometry to more accurately reflect actual crystal dimensions and extend the simulation to account for thermal transport effects.

4. Conclusions

In conclusion, the results obtained from SEM, X-ray analysis, and Raman spectroscopy demonstrate the feasibility of using the radio-frequency magnetron sputtering method to produce β -Ga₂O₃ films on silicon substrates. Gallium oxide films with a thickness of 250 nm and good crystallographic quality were obtained, as confirmed by comparison with literature data.

Raman spectra of the obtained films contain peaks in all three fundamental frequency regions (low-, medium-, and high-frequency) characteristic of β -Ga₂O₃. Together with the close agreement of the experimental XRD peaks with reference data for bulk crystals, this confirms that the deposited films correspond to the β -phase of Ga₂O₃ and possess sufficiently good crystalline quality. At the same time, the limited number of well-defined Raman peaks suggests that additional optimization of the deposition process could further improve film quality.

Raman spectroscopy in this study was employed for confirmation of the β -phase in $\mathrm{Ga_2O_3}$ films and for qualitative structural assessment, whereas stress evaluation was based on XRD and finite element method (FEM) modeling.

The experimental data suggest that further improvements in the RF magnetron sputtering technique, along with the incorporation of buffer layers between the Si substrate and the Ga_2O_3 film, could enable the fabrication of Ga_2O_3 films with minimal residual mechanical stress. X-ray analysis yielded stress values of ≈ 0.2 GPa in the $\beta\text{-}Ga_2O_3/\text{Si}$ structures, while numerical modeling estimated theoretical stresses of 0.22 GPa. The minor discrepancies between these values can be attributed to the presence of defects in the $\beta\text{-}Ga_2O_3$ film.

Overall, the measured stress values were consistent with or slightly lower than those in our previous work and those reported in the literature. Our finding indicates that the use of Si(111) substrates can eliminate the need for additional porous layers, thereby simplifying the fabrication process while maintaining favorable stress characteristics.

Better agreement between theoretical and experimental results may be achieved by accounting for heat transfer during the growth and cooling stages. A more comprehensive approach to XRD analysis is also required. In addition, employing the nanoindentation method is a promising approach for further mechanical characterization. Another important aspect for future investigation is the possible influence of silicon doping on strain formation in β -Ga₂O₃/Si heterostructures.

The presented results open a potential direction for researching the possibility of using the inexpensive RF magnetron sputtering technology and well-studied available silicon substrates to obtain high-quality β -Ga₂O₃ samples, which is an attractive material for modern semiconductor applications.

Further studies are planned to investigate the influence of the substrate characteristics and technological parameters of RF magnetron sputtering on the properties of β -Ga₂O₃/Si films.

Acknowledgments

A. Revenko acknowledges funding from the Science Foundation Ireland under the Supplemental Grant for Displaced Researchers scheme (SFI 20/FFP-P/8728 (S)). This research was also supported by the German Research Foundation under the Walter Benjamin Programme, referenced as KI 2865/1-1 (Valerii Kidalov).

References

- C.-H. Hsieh, L.-J. Chou, G.-R. Lin, Y. Bando, D. Golberg, *Nano Lett.* 8, 3081 (2008).
- [2] M. Higashiwaki, K. Sasaki, A. Kuramata, T. Masui, S. Yamakoshi, *Phys. Status Solidi A* 211, 21 (2014).
- [3] S. Fujita, Jpn. J. Appl. Phys. **54**, 030101 (2015).
- [4] X. Tang, X. Huang, Y. Huang et al., ACS Appl. Mater. Interfaces 10, 5519 (2018).
- [5] C. Baban, Y. Toyoda, M. Ogita, *Thin Solid Films* 484, 369 (2005).
- [6] A.V. Almaev, E.V. Chernikov, B.O. Kushnarev, N.N. Yakovlev, J. Phys. Conf. Ser. 1410, 012201 (2019).
- [7] M. Fleischer, H. Meixner, Sens. Actuators B 6, 257 (1992).
- [8] M. Higashiwaki, K. Sasaki, T. Kamimura, M.H. Wong, D. Krishnamurthy, A. Kuramata, T. Masui, S. Yamakoshi, Appl. Phys. Lett. 103, 123511 (2013).
- [9] G. Atmaca, H.-Y. Cha, Phys. Scr. 99, 035901 (2024).
- [10] C.-Y. Liu, Y.-B. Wang, X.-L. Jia et al., Phys. Scr. 99, 105931 (2024).
- [11] M. Higashiwaki, K. Sasaki, A. Kuramata, T. Masui, S. Yamakoshi, *Appl. Phys. Lett.* 100, 013504 (2012).
- [12] M.K. Yadav, A. Mondal, S. Shringi, S.K. Sharma, A. Bag, Semicond. Sci. Technol. 35, 085009 (2020).
- [13] X. Ji, J. Wang, S. Qi et al., J. Semicond. 45, 042503 (2024).
- [14] A. Kaya, H. Mao, J. Gao, R.V. Chopdekar, Y. Takamura, S. Chowdhury, M.S. Islam, *IEEE Trans. Electron Devices* 64, 2047 (2017).

- [15] A. Pérez-Tomás, E. Chikoidze, Y. Dumont et al., *Mater. Today Energy* 14, 100350 (2019).
- [16] T.G. Allen, A. Cuevas, Phys. Status Solidi RRL 9, 220 (2015).
- [17] T.G. Allen, A. Cuevas, *Appl. Phys. Lett.* **105**, 031601 (2014).
- [18] A.K. Chandiran, N. Tetreault, R. Humphry-Baker, F. Kessler, E. Baranoff, C. Yi, M.K. Nazeeruddin, M. Grätzel, Nano Lett. 12, 3941 (2012).
- [19] T. Oshima, T. Okuno, S. Fujita, Jpn. J. Appl. Phys. 46, 7217 (2007).
- [20] E.G. Villora, K. Shimamura, K. Kitamura, K. Aoki, Appl. Phys. Lett. 88, 031105 (2006).
- [21] A. Luchechko, V. Vasyltsiv, L. Kostyk, O. Tsvetkova, Acta Phys. Pol. A 133, 811 (2018).
- [22] M. Peres, E. Nogales, B. Mendez, K. Lorenz, M.R. Correia, T. Monteiro, N.B. Sedrine, ECS J. Solid State Sci. Technol. 8, Q3097 (2019).
- [23] S.B. Anooz, R. Grüneberg, T.-S. Chou et al., *J. Phys. D: Appl. Phys.* **54**, 034003 (2020).
- [24] V.I. Nikolaev, S.I. Stepanov, A.I. Pechnikov, S.V. Shapenkov, M.P. Scheglov, A.V. Chikiryaka, O.F. Vyvenko, ECS J. Solid State Sci. Technol. 9, 045014 (2020).
- [25] C.-H. Lin, K. Ema, S. Masuya, Q.T. Thieu, R. Sakaguchi, K. Sasaki, A. Kuramata, *Jpn. J. Appl. Phys.* **62**, SF1005 (2023).
- [26] K. Sasaki, A. Kuramata, T. Masui, E.G. Víllora, K. Shimamura, S. Yamakoshis, Appl. Phys. Expres 5, 035502 (2012).
- [27] H. Okumura, M. Kita, K. Sasaki, A. Kuramata, M. Higashiwaki, J.S. Speck, Appl. Phys. Express 7, 095501 (2014).
- [28] F. Alema, B. Hertog, A. Osinsky, P. Mukhopadhyay, M. Toporkov, W.V. Schoenfeld, J. Cryst. Growth 475, 77 (2017).
- [29] Y. Zhuo, Z. Chen, W. Tu, X. Ma, Y. Pei, G. Wang, Appl. Surf. Sci. 420, 802 (2017).
- [30] M. Orita, H. Ohta, M. Hirano, H. Hosono, Appl. Phys. Lett. 77, 4166 (2000).
- [31] F.-P. Yu, S.-L. Ou, D.-S. Wuu, *Opt. Mater. Express* **5**, 1240 (2015).
- [32] Z. Zhang, P. Yan, Q. Song, H. Chen, W. Zhang, H. Yuan, F. Du, D. Liu, D. Chen, Y. Zhang, Fundam. Res. 4, 1292 (2023).
- [33] H. Takane, K. Kaneko, Y. Ota, S. Fujita, Jpn. J. Appl. Phys. **60**, 055501 (2021).

- [34] Y. Zhang, J. Yan, Q. Li, C. Qu, L. Zhang, W. Xie, *Mater. Sci. Eng. B* 176, 846 (2011).
- [35] T. Kusaba, P. Sittimart, Y. Katamune et al., Appl. Phys. Express 16, 105503 (2023).
- [36] Z.-H. Chen, Y.-S. Wang, N. Zhang et al., *Chin. Phys. B* **32**, 017301 (2023).
- [37] J. Liang, D. Takatsuki, M. Higashiwaki, Y. Shimizu, Y. Ohno, Y. Naga, N. Shigekawa, Jpn. J. Appl. Phys. 61, SF1001 (2022).
- [38] Y. Oshima, E.G. Víllora, K. Shimamura, *Appl. Phys. Express* 8, 055501 (2015).
- [39] V.V. Kidalov, A.F. Dyadenchuk, V.P. Kladko, O.I. Gudymenko, M.P. Derhachov, S.O. Popov, O.O. Sushko, V.V. Kidalov, ECS J. Solid State Sci. Technol. 11, 025004 (2022).
- [40] C.-C. Yen, T.-M. Huang, P.-W. Chen, K.-P. Chang, W.-Y. Wu, D.-S. Wuu, ACS Omega 6, 29149 (2021).
- [41] S. Ayyuby, A. Kaur, S. Dhar, S. Mahapatra, *Proc. SPIE* 13367, 133670D (2025).
- [42] D. Guo, Q. Guo, Z. Chen, Z. Wu, P. Li, W. Tang, *Mater. Today Phys.* 11, 100157 (2019).
- [43] S.J. Pearton, J. Yang, P.H. Cary IV, F. Ren, J. Kim, M.J. Tadjer, M.A. Mastro, Appl. Phys. Rev. 5, 011301 (2018).
- [44] S. Husain, A.O.A. Keelani, *Mater. Today Proc.* 5, 5615 (2018).
- [45] Y.T. Prabhu, K.V. Rao, V.S.S. Kumar, B.S. Kumari, World J. Nano Sci. Eng. 4, 21 (2014).
- [46] A.S. Grashchenko, S.A. Kukushkin, V.I. Nikolaev, A.V. Osipov, E.V. Osipova, I.P. Soshnikov, *Phys. Solid State* 60, 852 (2018).
- [47] A.V. Osipov, A.S. Grashchenko, S.A. Kukushkin, V.I. Nikolaev, E.V. Osipova, A.I. Pechnikov, I.P. Soshnikov, Continuum Mech. Thermodyn. 30, 1059 (2018).
- [48] Y. Hara, W. Zhu, G. Deng, E. Marin, Q. Guo, G. Pezzotti, J. Phys. D Appl. Phys. 56, 125102 (2023).
- [49] A.V. Osipov, S.S. Sharofidinov, E.V. Osipova, A.V. Kandakov, A.Y. Ivanov, S.A. Kukushkin, *Coatings* 12, 1802 (2022).
- [50] H.Z. Zhang, Y.C. Kong, Y.Z. Wang et al., Solid State Commun. 109, 677 (1999).

- [51] S.A. Kukushkin, A.V. Osipov, J. Phys. D Appl. Phys. 47, 313001 (2014).
- [52] C. Kranert, C. Sturm, R. Schmidt-Grund, M. Grundmann, Sci. Rep. 6, 35964 (2016).
- [53] Y.C. Choi, W.S. Kim, Y.S. Park et al., Adv. Mater. 12, 746 (2000).
- [54] Y.H. Gao, Y. Bando, T. Sato, Y.F. Zhang, X.Q. Gao, Appl. Phys. Lett. 81, 2267 (2002).
- [55] R. Rao, A.M. Rao, B. Xu, J. Dong,
 S. Sharma, M.K. Sunkara, J. Appl. Phys.
 98, 094312 (2005).
- [56] N. Hasuike, I. Maeda, S. Isaji, K. Kobayashi, K. Ohira, T. Isshiki, Jpn. J. Appl. Phys. 62, SF1020 (2023).
- [57] D. Dohy, G. Lucazeau, A. Revcolevschi, J. Solid State Chem. 45, 180 (1982).
- [58] D. Machon, P.F. McMillan, B. Xu, J. Dong, Phys. Rev. B 73, 094125 (2006).
- [59] V.V. Kidalov, A.S. Revenko, D. Duleba, R.A. Redko, M. Assmann, A.I. Gudimenko, R.P. Johnson, ECS J. Solid State Sci. Technol. 13, 114003 (2024).
- [60] A.S. Gusev, N.I. Kargin, S.M. Ryndya, G.K. Safaraliev, N.V. Siglovaya, M.O. Smirnova, I.O. Solomatin, A.O. Sultanov, A.A. Timofeev, *Tech. Phys.* 66, 869 (2021).
- [61] M. Higashiwaki, K. Sasaki, H. Murakami, Y. Kumagai, A. Koukitu, A. Kuramata, T. Masui, S. Yamakoshi, Semicond. Sci. Technol. 31, 034001 (2016).
- [62] F. Orlandi, F. Mezzadri, G. Calestani, F. Boschi, R. Fornari, Appl. Phys. Express 8, 111101 (2015).
- [63] K. Adachi, H. Ogi, N. Takeuchi, N. Nakamura, H. Watanabe, T. Ito, Y. Ozaki, J. Appl. Phys. 124 085102 (2018).
- [64] J.J. Wortman, R.A. Evans, J. Appl. Phys. **36**, 153 (1965).
- [65] J. Vanhellemont, A.K. Swarnakar, O. Van der Biest, ECS Trans. 64, 283 (2014).
- [66] I. Henins, J. Res. Natl. Bur. Stand. A Phys. Chem. **68A**, 529 (1964).
- [67] H. Mukaida, H. Okumura, J.H. Lee, H. Daimon, E. Sakuma, S. Misawa, K. Endo, S. Yoshida, J. Appl. Phys. 62, 254 (1987).